COBEM 2023 27TH INTERNATIONAL CONGRESS OF MECHANICAL ENGENEERING

ABCM Brazilian Society of Mechanical Sciences and Engineering
27th ABCM International Congress of Mechanical Engineering
December 04-08, 2023, Florianópolis-SC, Brazil

COB-2023-1671
NUMERICAL SIMULATION OF DRUG TRANSPORT FROM DRUG-ELUTING STENTS THROUGH THE ARTERIAL WALL WITH AN ATHEROMA PLAQUE

H. Rosman
H. H. Shin
R. M. Lucena
J. Pontes
N. Mangiavacchi
Rio de Janeiro State University, Rio de Janeiro, RJ, Brazil
haroldo.rrj@gmail.com, hshin@pol.una.py, rachel.lucena@eng.uerj.br, norberto@eng.uerj.br, jose.pontes@uerj.br

S. McGinty
Division of Biomedical Engineering, University of Glasgow, Glasgow, UK
sean.mcginty@glasgow.ac.uk

Abstract. *Drug-eluting stents (DES) are widely used for treating coronary artery disease, but there are cases where restenosis and late stent thrombosis occur. In this context, understanding the effects of the drugs used in DES and the transport through the arterial wall on the overall health of DES-treated arteries presents a complex challenge that could be addressed through the development of mathematical and computational models. Although experimental efforts have been made to determine fundamental physical and biophysical parameters, these parameter values are not always applicable in all circumstances, particularly when atheroma plaque is present. In this context, this study performs a sensitivity analysis of transport parameters associated with atheroma plaque in arterial walls treated with DES. The drug elution from the polymer coating and its transport using advection-diffusion-reaction equations in the arterial wall are simulated on a 2D-axisymmetric unstructured grid, representing a portion of a DES with the adjacent arterial wall, using the Finite Element Method. The polymer layer of the DES and the arterial wall are modeled as porous media with incompressible flow and a constant pressure Dirichlet condition. A nonlinear dissolution model is used for the drug dynamics in the polymer coating, and a nonlinear saturable binding model that includes both specific and non-specific binding as separate phases in the arterial wall. The transport of the drug in the arterial wall is modeled considering an anisotropic diffusion tensor, with principal directions re-oriented in the vicinity of the stent to properly account for the compression and realignment of tissue fibers. Finally, the atheroma plaque is represented by the variation of permeability from its value in the arterial wall, using a hyperbolic tangent function to define a smooth artery/atheroma interface. The sensitivity analysis is performed by considering two types of atheroma plaque: soft and firm, using the drug sirolimus represented by literature parameters. The velocity field in the case of a firm atheroma is lower in magnitude compared to the normal arterial wall, which also reduces the convective transport of eluted drug. On the other hand, in the case of a soft atheroma, velocities are higher than in the normal arterial wall, resulting in an increased convective flux and, eventually, the wash out of the drug. The presence of either firm or soft atheromas significantly modifies the concentration distribution, possibly leading to the need for modified dosages and polymer formulations to compensate for these effects.*

Keywords: *drug-eluting stents, atheroma plaque, Darcy's law, convection-diffusion-reaction equations, Finite Element Method*

1. INTRODUCTION

Drug-eluting stents (DES) are small metal mesh tubes coated with a polymer that serve the purpose of keeping obstructed coronary arteries open. They are designed to facilitate the controlled release of medication, which aids in the healing of the damaged arterial wall (Cao *et al.*, 2021). Although drug-eluting stents (DES) are extensively employed in the treatment of coronary artery disease, concerns persist regarding the increased risk of in-stent restenosis (Dangas *et al.*, 2010; Giacoppo *et al.*, 2023) and late stent thrombosis (Camenzind *et al.*, 2007; Stone *et al.*, 2007). Thus, there are efforts to advance into a more effective and safe medical device in the treatment of coronary artery diseases (Cao *et al.*, 2021; Tan *et al.*, 2023; Yin *et al.*, 2023). At the same time, mathematical and computational modelling has also been advancing in the more accurate representation of the drug-eluting kinetics and the drug transport in the arterial wall vicinity of the implanted stent (Bozsak *et al.*, 2014; Lucena *et al.*, 2018; Frazzoli, 2020; Escuer *et al.*, 2022).

The coronary artery diseases are caused mainly by atherosclerosis with presence of atheromas plaques (calcified

fibrous materials, lipid, and cells) inside the arterial wall (Buja, 2015; Oikonomou *et al.*, 2018). These plaques can significantly modify the drug-delivery from stents through the arterial wall (Guo *et al.*, 2013). Thus, a model for the drug transport through the atheroma plaques needs to be considered in order to obtain adequate simulation results for evaluating safety and efficacy of a DES.

Soft atheroma plaques consist of a lipid-rich core covered by a fibrous cap, while hard plaques contain additional calcium deposits, making them more rigid and less elastic, and resulting in reduced permeability. Ferreira *et al.* (2018), for instance, models a calcified atheroma cap as having zero permeability. Transition from soft to hard plaques can occur, and the permeability of plaques can evolve over time depending on their specific characteristics and stages.

Although there have been publications discussing the physicochemical properties of certain drugs associated with atheroma plaques (Hossain *et al.*, 2012; Guo *et al.*, 2013), determining precise parameter values is often challenging due to inter-individual variations and the specific conditions during DES implantation (Tocci *et al.*, 2015). In this regard, conducting sensitivity analyses of these parameters using mathematical and computational models can provide valuable insights into the underlying biophysical phenomena. Such analyses can contribute to the development of safer and more effective drug-eluting stents (DES) by enhancing our understanding of these complex processes.

Therefore, this work focuses on the effect of the presence of atheroma plaque in the DES-treated arterial wall on the overall drug transport dynamics through the plaque and the arterial wall. The models used in this work are based on the modelling framework of Lucena *et al.* (2018). Lucena *et al.* (2018) considered a 2d-axisymmetric geometry of a portion of a DES with the adjacent arterial wall, and the model equations were solved using the Finite Element Method. The polymer layer of DES and the arterial wall were modelled as porous media with incompressible flow and a constant pressure difference imposed across the arterial wall. The drug-elution and saturable specific and non-specific binding in the arterial wall were modelled as proposed by McGinty and Pontrelli (2015). Finally, an anisotropic diffusion tensor was included by Frazzoli (2020) into the aforementioned modeling framework in order to account for the compression and realignment of tissue fibers in the vicinity of the implanted stent, so the diffusion tensor has its principal directions re-oriented due to the presence of the stent.

This study builds upon the modelling framework proposed by Lucena *et al.* (2018) to include a drug transport model for atheroma plaques. The model incorporates a variation in permeability, represented by a hyperbolic tangent function at the smooth interface between the plaque and arterial wall. A sensitivity analysis is performed to account for different patient situations. Simulation results with varying permeabilities are compared to the findings of Lucena *et al.* (2018) and Frazzoli (2020) to enhance understanding of drug transport dynamics.

The proposed model and the numerical methods are presented in Section 2. Section 3shows the results obtained by the computer simulations, followed by some discussions. Finally, the conclusion of the work is presented in Section 4.

2. THE MATHEMATICAL MODEL AND NUMERICAL METHOD

In this section, the mathematical model (Section 2.1) and the numerical method (Section 2.2) employed for the computer simulations are presented.

2.1 Mathematical model

Figure 1(a) shows the 2d-axisymmetric domain composed of a polymer layer (Ω_1) covering a stent strut, and a portion of arterial wall (Ω_2) where the strut is half-embedded, and (b) shows a 3d sketch of the axisymmetric geometry of the problem. The axial direction coincides with the direction of the lumen, and the radial direction is chosen as orthogonal to the arterial wall. The dimension of the geometry is similar to the one used in Lucena *et al.* (2018): lumen radius $r_0 = 1.5$ mm, arterial wall thickness $L_r = r_{max} - r_0 = 0.5$ mm, stent strut diameter $d_s = 0.25$ mm, stent polymer thickness $L_p = 0.05$ mm, and the length of the arterial wall $L_z = 0.7$ mm. The endothelium near the polymer layer is considered denuded due to the lesion (Bozsak *et al.*, 2014), comprised by the length $L_s = 0.15$ mm on both sides adjacent to the embedded polymeric layer. Away from the polymer layer, the endothelium is considered intact.

The arterial wall is considered as a porous media, and the fluid (plasma) flow is modelled by Darcy's law and continuity equation:

$$\mathbf{u} = -\frac{1}{\mu} P_{Di} \nabla p, \qquad \text{in } \Omega_1 \cup \Omega_2, \text{ for } i = \{p, w\}, \tag{1}$$

$$\nabla \cdot \mathbf{u} = 0, \qquad \text{in } \Omega_1 \cup \Omega_2, \tag{2}$$

where $\mathbf{u} = (u_r, u_z)$ is the Darcy velocity field with radial and axial components, respectively, p is the pressure field, $\mu = 7.2 \times 10^{-4}$ Pa·s is plasma dynamic viscosity (Zunino, 2004), $P_{Dp} = 2.78 \times 10^{-21}$ m^2 is the permeability in the polymer layer, and P_{Dw} is the permeability in the arterial wall. In this work, the arterial wall is composed of injured atheroma with a thin transition to smooth muscle cells (SMC). Because there is no available information about the permeability in the atheroma, we consider values ten times larger and ten times smaller from the permeability in the SMC reported in the literature ($P^*_{Dw} = 2 \times 10^{-18}$ m^2, see Bozsak *et al.* (2014)) in order to perform the sensitivity analysis. A hyperbolic

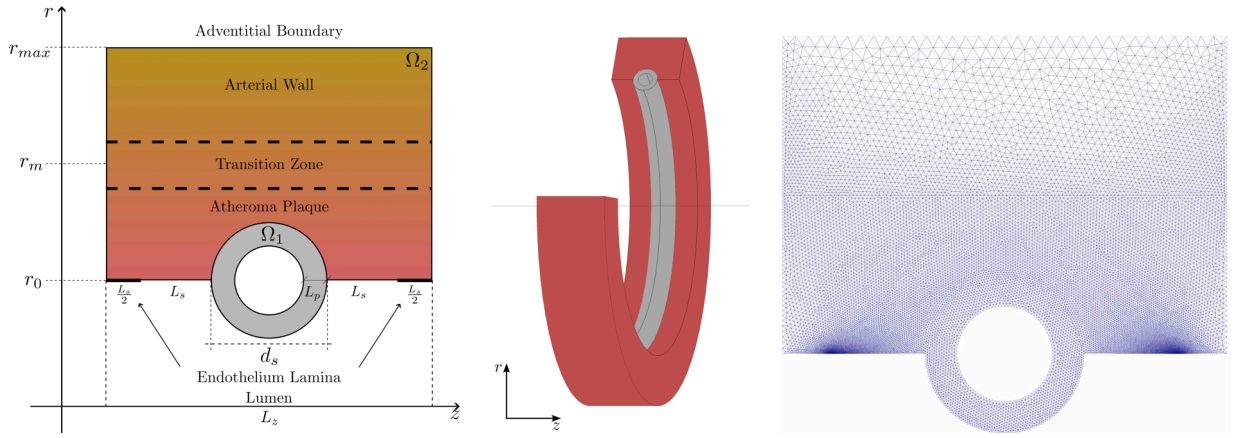

(a) (b) (c)

Figure 1. (a) Domain of 2d-axisymmetric geometry (Ω_1: polymer layer, Ω_2: arterial wall) with denuded endothelium in the vicinity of the stent. (b) Illustrative 3d sketch of the problem. (c) Computational domain and unstructured triangular mesh employed in the simulations.

tangent function is used to take into account the transition between atheroma and SMC. Therefore, the permeability in the arterial wall is expressed as a function of the radial axis as follows

$$P_{Dw}(r) = P^*_{Dw}\left[\frac{1}{2}(\gamma+1) + \frac{1}{2}(\gamma-1)\tanh\left(\frac{10\pi}{L_r}(r_m - r)\right)\right], \tag{3}$$

where r_m is the position of the transition which is considered at the middle of the arterial wall, the factor $L_r/10$ corresponds to the length scale of the transition thickness which is one-tenth of the arterial wall thickness, and γ is the ratio of the considered permeability in atheroma to the permeability in the SMC.

For the numerical solution of the equations (1) and (2), an overpressure of 9.31×10^3 Pa is prescribed on the lumen side of the boundary compared to the adventitial side (Ai and Vafai, 2006), and the periodic boundary condition is considered in the axial direction.

The transport of dissolved drug concentration, c, is modelled by the following advection-diffusion-reaction equations:

$$\frac{\partial c}{\partial t} + \mathbf{u}_p \cdot \nabla c = \nabla \cdot (\mathbf{D}_p \nabla c) + f_0(b_0, c), \qquad \text{in } \Omega_1 \text{ (polymer layer)}, \tag{4}$$

$$\frac{\partial c}{\partial t} + \mathbf{u}_w \cdot \nabla c = \nabla \cdot (\mathbf{D}_w \nabla c) - f_{ns}(b_{ns}, c) - f_s(b_s, c), \qquad \text{in } \Omega_2 \text{ (arterial wall)}, \tag{5}$$

where $\mathbf{u}_p = \mathbf{u}/\phi_p$ and $\mathbf{u}_w = \mathbf{u}/\phi_w$ are the seepage velocity in the polymer layer and arterial wall with its effective porosity $\phi_p = \phi_w = 0.29$, respectively (Bozsak *et al.*, 2014). $\mathbf{D}_p$ and $\mathbf{D}_w$ are the diffusivity tensor of the drug in the polymer layer and arterial wall, respectively, f_0 is the dissolution rate of the drug in the polymer layer from the solid concentration b_0, and f_{ns} and f_s are the rates of non-specifically and specifically bound drug kinetics, respectively, with non-specifically bound drug concentration b_{ns} and specifically bound concentration b_s. In this work, the data of transport and pharmacokinetic properties of sirolimus are employed. The diffusion coefficient of the sirolimus in the polymer layer is considered as homogeneous and isotropic, with the value equal to 10^{-14} m^2 s^{-1} (Bozsak *et al.*, 2014). In the arterial wall, the diffusion coefficient of the sirolimus drug in the radial direction is 7×10^{-12} m^2 s^{-1}, and in the axial direction is 4×10^{-11} m^2 s^{-1} (Bozsak *et al.*, 2014). These diffusion coefficients are the diagonal components of the orthotropic diffusivity $\mathbf{\Lambda}$.

Due to the stent implantation, the fibers of the arterial wall are deformed, and therefore, the transport properties of the eluted drug in the SMC are altered. In this context, Frazzoli (2020) considered a modified diffusivity tensor in the arterial wall due to the realignment of the fibers of the arterial tissue after the stent implantation. Thus, the diffusivity tensor $\mathbf{D}_w$ in the arterial wall is expressed in terms of the orthotropic diffusivity $\mathbf{\Lambda}$, using the similarity transformation by an orthogonal matrix $\mathbf{S}$ whose columns are composed by the principal directions: perpendicular and tangential directions of the fibers in the arterial wall, *i.e.*, $\mathbf{D}_w = \mathbf{S}\mathbf{\Lambda}\mathbf{S}^{-1}$.

An auxiliary potential function ϕ, with value zero on the adventitia and one on the deformed endothelium due to the embedded strut, is considered in order to obtain the principal directions of the fibers. Therefore, the potential function ϕ is obtained by solving the equation $\nabla^2\phi = 0$, and the perpendicular, $\mathbf{v}_\perp$, and tangential, $\mathbf{v}_\parallel$, directions of the fibers are computed, respectively, as following:

$$\mathbf{v}_\perp = \frac{\nabla\phi}{||\nabla\phi||} \qquad \text{and} \qquad \mathbf{v}_\parallel = \mathbf{R}_{\pi/2}\mathbf{v}_\perp. \tag{6}$$

In the last expressions, $\mathbf{R}_{\pi/2}$ is the rotation matrix which rotates the vector $\mathbf{v}_\perp$ counterclockwise through an angle $\pi/2$ about the origin, and $||\cdot||$ is the Euclidean norm.

The equation for the dissolution of the drug in the polymer layer is expressed as:

$$\frac{db_0}{dt} = -f_0(b_0, c) = -\beta_0\, b_0^{2/3}\,(S_0 - c)\,, \qquad \text{in } \Omega_1 \tag{7}$$

where $\beta_0 = 10^{-4}\ (\mathrm{mol\,m^{-3}})^{-2/3}\,\mathrm{s^{-1}}$ is the dissolution rate and $S_0 = 10\ \mathrm{mol\,m^{-3}}$ is the drug solubility (McGinty and Pontrelli, 2016). Furthermore, the equations of pharmacokinetics for the non-specifically bound and specifically bound drug concentrations are given, respectively, as:

$$\frac{db_{ns}}{dt} = f_{ns}(b_{ns}, c) = k_{ns}^f\, c\,(b_{ns}^{max} - b_{ns}) - k_{ns}^r\, b_{ns}, \qquad \text{in } \Omega_2 \tag{8}$$

$$\frac{db_s}{dt} = f_s(b_s, c) = k_s^f\, c\,(b_s^{max} - b_s) - k_s^r\, b_s, \qquad \text{in } \Omega_2 \tag{9}$$

where $b_{ns}^{max} = 0.363\ \mathrm{mol\,m^{-3}}$ and $b_s^{max} = 3.3 \times 10^{-3}\ \mathrm{mol\,m^{-3}}$ are the saturations values of non-specifically and specifically bound drug concentration, $k_{ns}^f = 2\ (\mathrm{mol\,m^{-3}\,s})^{-1}$ and $k_s^f = 800\ (\mathrm{mol\,m^{-3}\,s})^{-1}$ are the rate constant of binding kinetics, and $k_{ns}^r = 5.2 \times 10^{-3}\ \mathrm{s^{-1}}$ and $k_s^r = 1.6 \times 10^{-4}\ \mathrm{s^{-1}}$ are the unbinding rates of the bound drug concentration (McGinty and Pontrelli, 2016).

In the region Ω_2, the initial conditions for the free concentration c, specifically bound concentration b_s, and non-specifically bound concentration b_{ns} are all set to zero. On the other hand, in the region Ω_1, the undissolved concentration b_0 is initialized to a value of $100\ \mathrm{mol\,m^{-3}}$ (Bozsak *et al.*, 2014).

2.2 Numerical method

A finite element package based on the Julia just-in-time (JIT) compiler (Badia and Verdugo, 2020; Verdugo and Badia, 2022) is employed for the resolution of the governing equations in two-dimensional axisymmetric coordinates.

The weak form for the Darcy's law is:

$$\int_{\Omega_1} P_{D_p}(\nabla p)\cdot(\nabla q)\,d\Omega + \int_{\Omega_2} P_{D_w}(\nabla p)\cdot(\nabla q)\,d\Omega = 0, \tag{10}$$

where q is the weighting function belonging to the Sobolev space with square-integrable first derivative. The resulting linear system is solved using LU factorization.

With the obtained pressure, the velocity field is obtained using the weak form of the Eq. (1):

$$\int_{\Omega_1\cup\Omega_2} \mathbf{u}\cdot\mathbf{v}\,d\Omega = -\frac{1}{\mu}\int_{\Omega_1} P_{D_p}(\nabla p)\cdot\mathbf{v}\,d\Omega - \frac{1}{\mu}\int_{\Omega_2} P_{D_w}(\nabla p)\cdot\mathbf{v}\,d\Omega, \tag{11}$$

where $\mathbf{v}$ is the weighting function belonging to the vector-valued Sobolev space with square-integrable first derivative. The subsequent linear system is also solved using LU factorization.

The transport equations are solved using first order implicit time-stepping method for the advection-diffusion terms and Newton-Raphson method for the convergence of inner fractional-stepping of the reaction terms. Thus, the weak form of the transport equations is expressed as:

$$\int_{\Omega_1\cup\Omega_2} \frac{c_*^{n+1} - c^n}{\Delta t} q\,d\Omega + \int_{\Omega_1} (\mathbf{u}_p\cdot\nabla c_*^{n+1}) q\,d\Omega + \int_{\Omega_2} (\mathbf{u}_w\cdot\nabla c_*^{n+1}) q\,d\Omega + \int_{\Omega_1} (\mathbf{D}_p\nabla c_*^{n+1})\cdot(\nabla q)\,d\Omega + \int_{\Omega_2} (\mathbf{D}_w\nabla c_*^{n+1})\cdot(\nabla q)\,d\Omega = 0, \tag{12}$$

where c^n is the known concentration field at time $t_n = n\Delta t$, and c_*^{n+1} is the concentration in the new time-step without the contribution of the reaction terms.

The Newton-Raphson method is employed to solve the non-linear equations emerged when reaction terms are taken into account. As the reactions terms considered in this work are mass conservative, the time advancement of the drug dissolution in the polymer layer (Ω_1):

$$\frac{b_0^{n+1} - b_0^n}{\Delta t} = -f_0(b_0^{n+1}, c^{n+1}), \qquad \text{in } \Omega_1, \tag{13}$$

is combined with the correction of the concentration $c^{n+1} - c_*^{n+1} = -b_0^{n+1} + b_0^n$ in Ω_1, obtaining the following equation:

$$\frac{b_0^{n+1} - b_0^n}{\Delta t} = -f_0(b_0^{n+1}, c_*^{n+1} - b_0^{n+1} + b_0^n), \qquad \text{in } \Omega_1. \tag{14}$$

Similarly, the advancement of the binding reactions in the arterial wall is combined with $c^{n+1} - c_*^{n+1} = -b_{ns}^{n+1} + b_{ns}^n - b_s^{n+1} + b_s^n$ in Ω_2, which return the following set of equations:

$$\frac{b_{ns}^{n+1} - b_{ns}^n}{\Delta t} = f_{ns}(b_{ns}^{n+1}, c_*^{n+1} - b_{ns}^{n+1} + b_{ns}^n - b_s^{n+1} + b_s^n), \qquad \text{in } \Omega_2, \tag{15}$$

$$\frac{b_s^{n+1} - b_s^n}{\Delta t} = f_s(b_s^{n+1}, c_*^{n+1} - b_{ns}^{n+1} + b_{ns}^n - b_s^{n+1} + b_s^n), \qquad \text{in } \Omega_2. \tag{16}$$

3. COMPUTATIONAL RESULTS AND DISCUSSION

3.1 Computational set-up

The computational mesh used in this work is an unstructured triangular mesh with 38,187 triangular elements and 114,561 nodes (see Fig. 1(c)). The second order triangular elements are employed. The regions with larger gradients of the variables were refined, thus, grid-independence was achieved. The temporal step for the transient simulation is $\Delta t = 50$ s, and it is extended until $t_f = 20$ days after the stent implantation at $t_0 = 0$.

Three sets of simulations are performed (see Table from Fig. 2(a)). The default case with identification `ath0` considers the SMC without atheroma, hence the permeability in the arterial wall is not modified, which is given by $\gamma = 1.0$; this is the configuration used in Lucena *et al.* (2018) and Frazzoli (2020). The other two cases consider the presence of atheroma plaque: (i) larger permeability for the atheroma plaque with $\gamma = 10.0$ (simulation identification `ath+`), and (ii) lower permeability for the atheroma plaque with $\gamma = 0.1$ (simulation identification `ath-`). Figure 2(b) shows the sketch of the domain with two line segments in the radial direction $\overline{\text{A'A"}}$ and $\overline{\text{B'B"}}$ where the variables fields are computed and compared between the results of the simulated cases.

Simulation ID	Permeability ratio γ
`ath0`	1.00
`ath+`	10.0
`ath-`	0.10

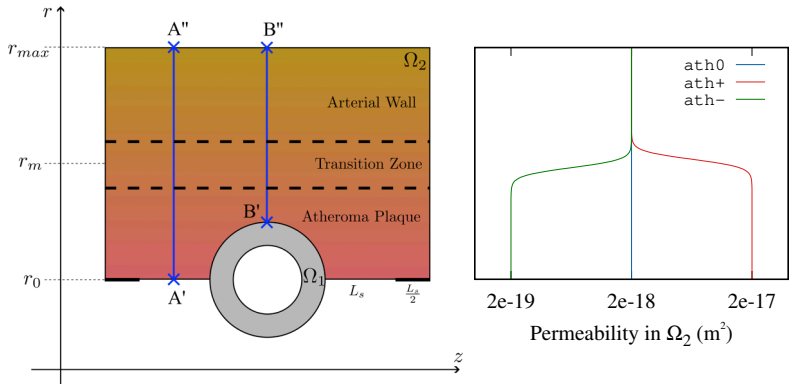

(a) (b) (c)

Figure 2. (a) Detail of the simulations performed. (b) Domain with two line segments $\overline{\text{A'A"}}$ and $\overline{\text{B'B"}}$ where the variables fields are computed. (c) Permeability distribution of the simulated cases, with its vertical axis aligned along the radial direction of the figure (b).

3.2 Pressure and velocity fields

The pressure fields from the simulation results are presented in Fig. 3. In the case with higher permeability (case `ath+`), Fig. 3(b) shows that the arterial wall is exposed to higher pressure and larger gradients in SMC; on the contrary, larger gradients are observed in the atheroma plaque with lower pressure in the SMC in case of lower permeability for the atheroma (case `ath-`). This can also be observed in Fig. 5(a), where the pressure fields are computed over the line segments $\overline{\text{A'A"}}$ and $\overline{\text{B'B"}}$.

As a result of the effect of the atheroma on the pressure field, the velocity field is accordingly altered, as shown in Fig. 4. A higher permeability of the atheroma plaque (`ath+`) is correlated with a higher velocity in the arterial wall, exhibiting approximately an order of magnitude difference in velocity compared to the absence of atheroma (`ath0`). Figure 5(b) shows the velocity magnitude computed over the line segments $\overline{\text{A'A"}}$ and $\overline{\text{B'B"}}$; there are differences in the order of magnitude of the velocity between the cases simulated. The presence of the embedded stent reduces drastically the velocity in the arterial wall above the polymer (see the dashed lines in Fig. 5(b)).

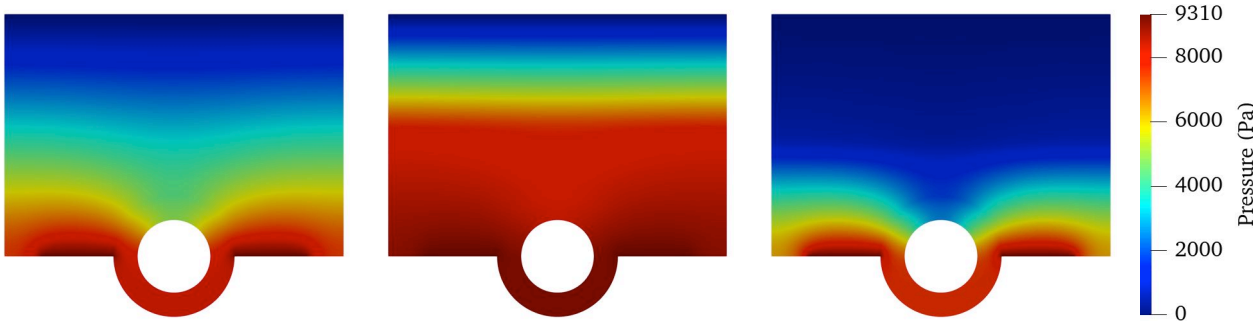

(a) `ath0` (b) `ath+` (c) `ath-`

Figure 3. Pressure fields considering no atheroma and two different cases of atheroma plaque.

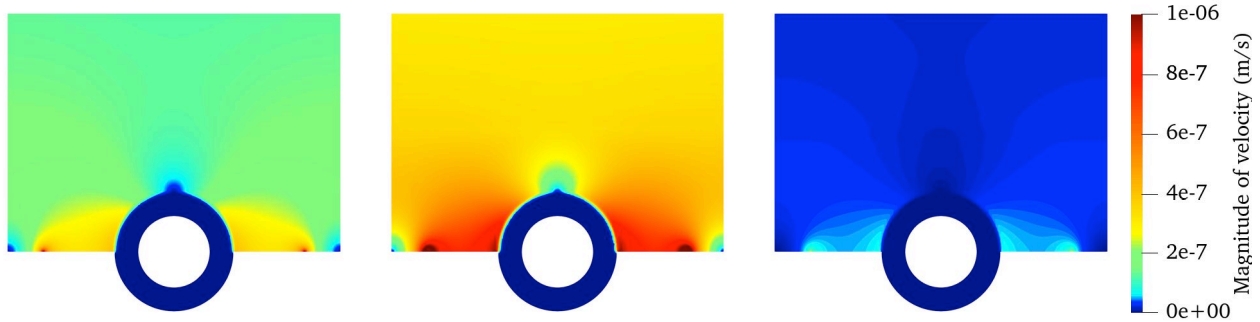

(a) `ath0` (b) `ath+` (c) `ath-`

Figure 4. Magnitude of seepage velocity.

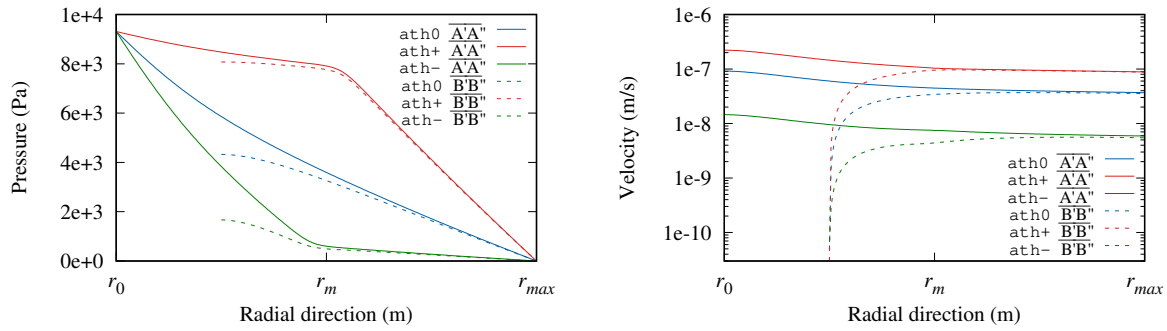

(a) Pressure (b) Velocity

Figure 5. Pressure and magnitude of seepage velocity computed over the line segments $\overline{\text{A'A"}}$ and $\overline{\text{B'B"}}$.

3.3 Drug concentration fields

Figure 6 shows the concentration field corresponding to the second day after the stent implantation. In all simulated cases, the specifically bound drug b_s is saturated at $t = 2$ days, so the figures showing the distribution of the b_s were not presented because they do not give relevant information for our discussion.

The Péclet number in the radial direction is defined as $\text{Pe}_r = L_r\, u/D$, where L_r is the arterial wall thickness, u is the representative velocity in the radial direction, and D the diffusion coefficient of the eluted drug in the arterial wall in the radial direction. This Péclet number is in the order of 3.5 in the default case `ath0`, and 7.0 and 0.6 in the cases with atheroma plaque `ath+` and `ath-`, respectively. This means that the transport of the eluted drug in the cases `ath0` and `ath+` are dominated by the advection, and it is slightly dominated by the diffusion in the case `ath-`.

The dominance of advection or diffusion in the transport of the eluted drug has a significant impact on its distribution and availability within the arterial wall. This effect is evident in Fig. 6, where the concentration fields of the drug (c) and non-specifically bound drug (b_{ns}) on the second day after stent implantation are depicted. In the case of `ath-`, where diffusion primarily governs the transport process, a sufficiently high concentration of the drug is present in most regions of the arterial wall, facilitating binding. However, there is still a noticeable concentration of the drug remaining primarily

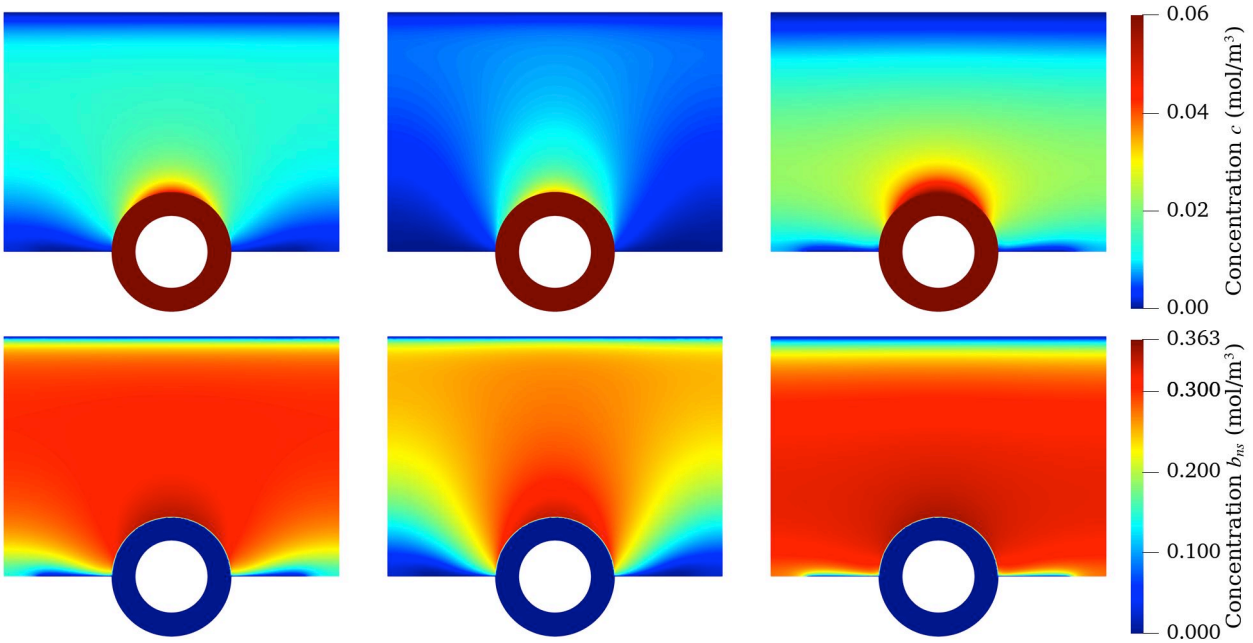

(a) `ath0` (b) `ath+` (c) `ath-`

Figure 6. Concentration c and b_{ns} on second day after the stent implantation.

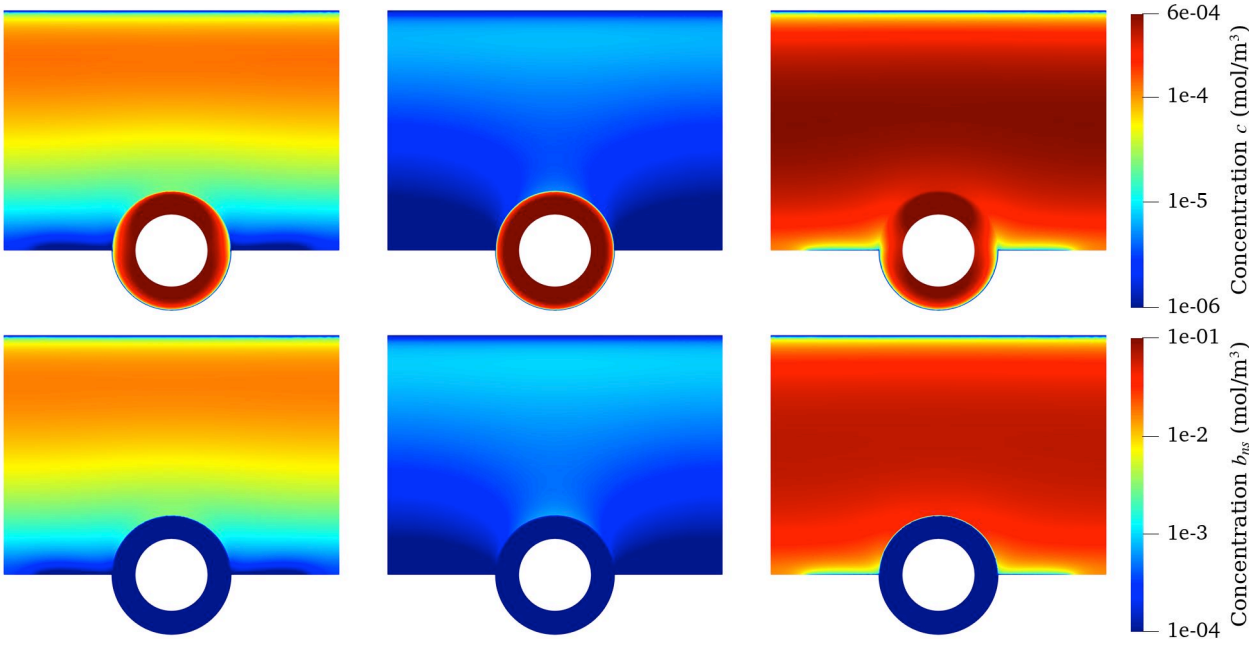

(a) `ath0` (b) `ath+` (c) `ath-`

Figure 7. Concentration c and b_{ns} on twentieth day after the stent implantation.

in the areas where the atheroma plaque is located. These concentration distributions are further demonstrated in the line plots shown in Fig. 8, which represent the computed concentrations along the line segments $\overline{\text{A'A"}}$ and $\overline{\text{B'B"}}$.

A concerning scenario arises when the transport of the eluted drug is heavily dominated by advection, as is the case in `ath+`. In such circumstances, an inadequate amount of drug concentration near the endothelium is available for binding. Indeed, in the vicinity of the endothelium, the eluted drug from the polymer layer must rely on diffusion to reach that region. However, in the case of `ath+`, the advection velocity in the radial direction significantly washes away the drug that is being transported by the diffusion process near the endothelium. Furthermore, in the case of `ath+`, the concentration (c) of the drug is, at most, three times lower compared to the concentration in `ath-`, and approximately half of the concentration compared to `ath0` (see the plots of Fig. 8). The distribution of the non-specifically bound drug in the case `ath+` is also lower compared to the cases `ath0` and `ath-`. Finally, larger concentration c is observed in SMC, away from the atheroma plaque in the cases `ath0` and `ath+`, on the contrary to the case `ath-`.

The distributions of the free concentration c and the concentration of non-specifically bound drug b_{ns} at $t = 20$ days after the stent implantation are shown in Fig. 7. On the twentieth day, the drug concentration (c) in all cases is significantly lower compared to the second day, reaching orders of magnitude decrease. Due to substantial variations among the simulated cases, logarithmic scaling has been employed for the color maps in the figure to effectively represent the differences spanning several orders of magnitude. The concentration c in the case `ath+` is several orders lower than the concentration in the case `ath-`, showing that the effect of the advection velocity is severe on the availability of the eluted drug in the arterial wall on the twentieth day. The concentration of the non-specifically bound drug b_{ns} in the case `ath+` is nearly two order of magnitudes lower compared to the concentration in the case `ath-`.

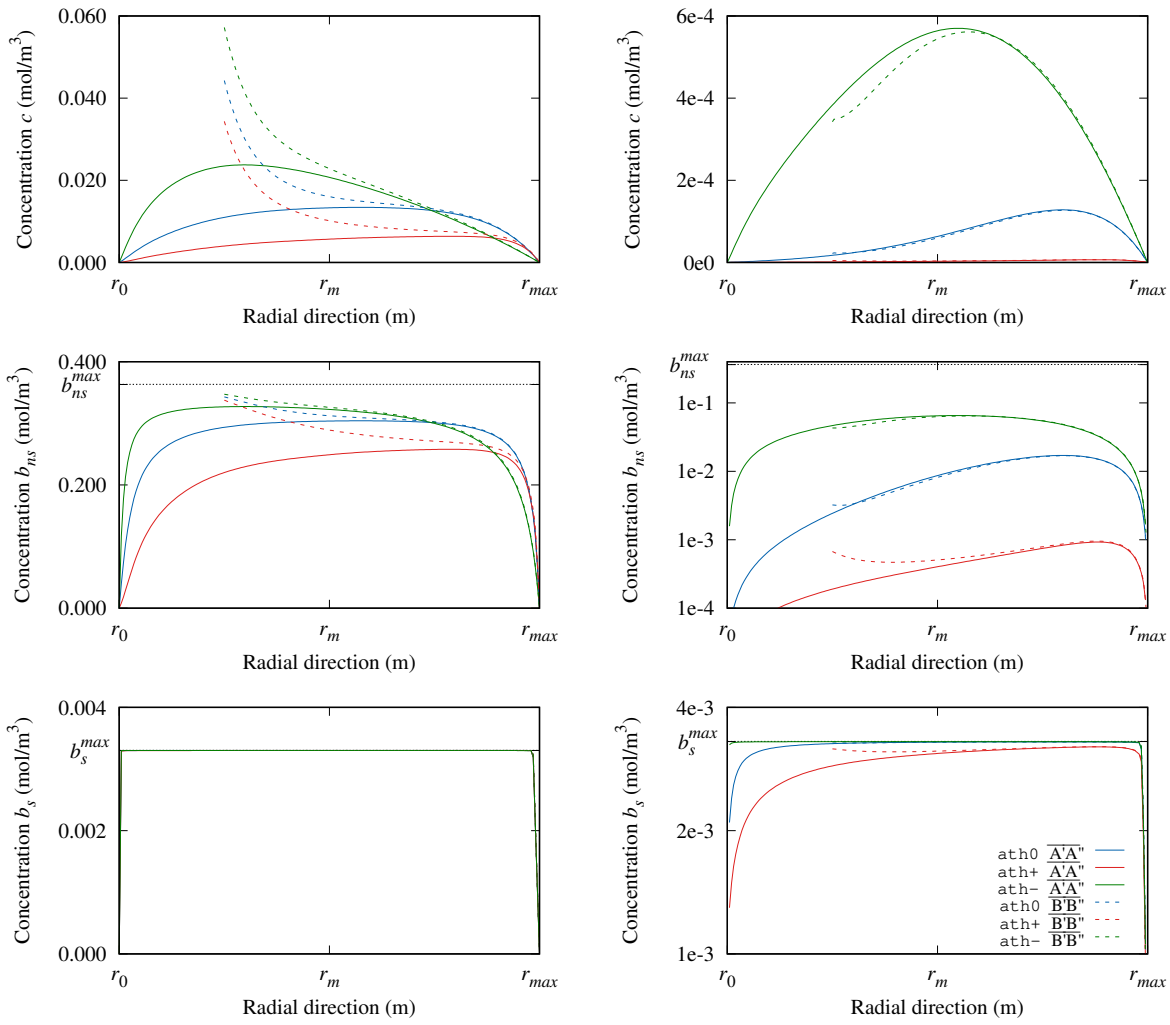

(a) $t = 2$ days (b) $t = 20$ days

Figure 8. Concentrations computed over the line segments $\overline{\text{A'A"}}$ and $\overline{\text{B'B"}}$.

The velocity in the polymer layer is several orders of magnitude lower compared to that in the arterial wall, due to the reduced permeability (at least in three orders of magnitude). Thus, the dissolved drug in the polymer layer is mainly transported by the diffusion process, so the decaying of the drug mass in the polymer layer does not depend on

the permeability of the atheroma. This can be observed in the average concentration along the time shown in Fig. 9(a). The concentration in the polymer layer begins with 100 mol m^{-3}, and a nearly exponential time decay is observed. The half-life in the first 10 days is roughly 3.5 days, and then it reduces to 15 hours.

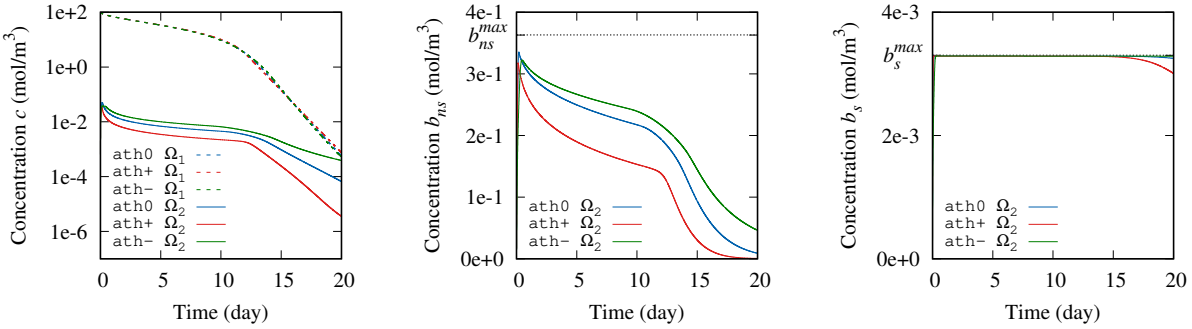

Figure 9. Average concentration along the time: (a) Concentration c, (b) concentration of non-specifically bound drug b_{ns}, and (c) concentration of specifically bound drug b_s.

The average concentration in the arterial wall, in the case `ath+`, is lower than the other two cases, and after the 10 days it decays more rapidly; on the contrary, more drug is retained in the arterial wall for longer time in the case `ath-`. Figure 9(b) shows the concentration of non-specifically bound drug b_{ns} in the arterial wall along the time. In all cases simulated in this study, saturation of the non-specifically bound drug throughout the entire arterial wall is not attained. However, in the case `ath-`, in average reaches higher binding compared to the case `ath+`. The average concentration of specifically bound drug b_s along the time is shown in Fig. 9(c). In all simulated cases, the saturation of specifically bound drug is reached; the case `ath+` starts to decay from about 15 days, while it is still maintained saturated in the case `ath-` on the twentieth day.

3.4 Limitations

This study, like any computational analysis, involves simplifications. The representation of the arterial wall, stent, and atheroma plaque is based on a simplified geometric model, which may not fully capture the complexities seen in individual patients. Atheroma plaques are known to exhibit significant heterogeneity, leading to variations in their properties. However, for this study, constant values were used for permeability, diffusivity, and porosity. We also assume a constant density of binding sites throughout the arterial wall, although in reality, the composition of atheroma and binding site density are expected to vary.

4. CONCLUSIONS

A sensitivity analysis is performed to determine the drug distribution in the arterial wall after the drug-eluted stent implantation based on changes in the permeability of the atheroma plaque. Data of transport properties of sirolimus drug is employed. Higher advection velocity and overall lower drug concentration in the arterial wall are observed for higher permeability in the atheroma plaque. On the contrary, lower advection velocity and higher drug concentration are present for lower permeability in the atheroma plaque. As a result, when the atheroma plaque has lower permeability, as in the case of hard atheromas, there is a greater availability of the drug in the arterial wall for an extended period of time.

The distribution of the eluted-drug in the arterial wall is highly dependent on the permeability value in the atheroma plaque. Thus, the precise characterization of the atheroma plaque is necessary for the desired response of the implanted drug-eluted stent.

5. ACKNOWLEDGEMENTS

The authors would like to acknowledge financial support from FAPERJ, CAPES, CNPq, and the University of Glasgow EPSRC GCF ISF fund.

6. REFERENCES

Ai, L. and Vafai, K., 2006. "A coupling model for macromolecule transport in a stenosed arterial wall". *International journal of heat and mass transfer*, Vol. 49, No. 9-10, pp. 1568–1591.

Badia, S. and Verdugo, F., 2020. "Gridap: An extensible finite element toolbox in Julia". *Journal of Open Source Software*, Vol. 5, No. 52, p. 2520.

Bozsak, F., Chomaz, J. and Barakat, A., 2014. "Modelling the transport drugs of eluted from stents: physical phenomena driving drug distribution in the arterial wall". *Biomech Model Mechanobiol*, Vol. 13, pp. 327–347.

Buja, L.M., 2015. "Coronary Artery Disease: Pathological Anatomy and Pathogenesis". In J.T. Willerson and D.R. Holmes Jr., eds., *Coronary Artery Disease*, Springer London, London, pp. 1–20.

Camenzind, E., Steg, P.G. and Wijns, W., 2007. "Stent thrombosis late after implantation of first-generation drug-eluting stents: A cause for concern". *Circulation*, Vol. 115, No. 11, pp. 1440–1455.

Cao, D., Chandiramani, R., Chiarito, M., Claessen, B.E. and Mehran, R., 2021. "Evolution of antithrombotic therapy in patients undergoing percutaneous coronary intervention: a 40-year journey". *European Heart Journal*, Vol. 42, No. 4, pp. 339–351.

Dangas, G.D., Claessen, B.E., Caixeta, A., Sanidas, E.A., Mintz, G.S. and Mehran, R., 2010. "In-Stent Restenosis in the Drug-Eluting Stent Era". *Journal of the American College of Cardiology*, Vol. 56, No. 23, pp. 1897–1907.

Escuer, J., Schmidt, A.F., Peña, E., Martínez, M.A. and McGinty, S., 2022. "Mathematical modelling of endovascular drug delivery: Balloons versus stents". *International Journal of Pharmaceutics*, Vol. 620, p. 121742.

Ferreira, J.A., Gonçalves, L., Naghipoor, J., de Oliveira, P. and Rabczuk, T., 2018. "The effect of plaque eccentricity on blood hemodynamics and drug release in a stented artery". *Medical engineering & physics*, Vol. 60, pp. 47–60.

Frazzoli, F.A.S., 2020. *Anisotropic transport through polymer layer and porous arterial wall with binding in drug-eluting stents using the FEM*. Master's thesis, Rio de Janeiro State University.

Giacoppo, D., Alvarez-Covarrubias, H.A., Koch, T., Cassese, S., Xhepa, E., Kessler, T., Wiebe, J., Joner, M., Hochholzer, W., Laugwitz, K.L., Schunkert, H., Kastrati, A. and Kufner, S., 2023. "Coronary artery restenosis treatment with plain balloon, drug-coated balloon, or drug-eluting stent: 10-year outcomes of the ISAR-DESIRE 3 trial". *European Heart Journal*.

Guo, J., Saylor, D.M., Glaser, E.P. and Patwardhan, D.V., 2013. "Impact of Artificial Plaque Composition on Drug Transport". *Journal of Pharmaceutical Sciences*, Vol. 102, No. 6, pp. 1905–1914.

Hossain, S.S., Hossainy, S.F.A., Bazilevs, Y., Calo, V.M. and Hughes, T.J.R., 2012. "Mathematical modeling of coupled drug and drug-encapsulated nanoparticle transport in patient-specific coronary artery walls". *Computational Mechanics*, Vol. 49, No. 2, pp. 213–242.

Lucena, R., Mangiavacchi, N., Pontes, J., Anjos, G. and McGinty, S., 2018. "On the transport through polymer layer and porous arterial wall in drug-eluting stents". *Journal of the Brazilian Society of Mechanical Sciences and Engineering*, Vol. 40, No. 572.

McGinty, S. and Pontrelli, G., 2016. "On the role of specific drug binding in modelling arterial eluting stents". *J Math Chem*, Vol. 54, pp. 967–976.

McGinty, S. and Pontrelli, G., 2015. "A general model of coupled drug release and tissue absorption for drug delivery devices". *Journal of Controlled Release*, Vol. 217, pp. 327–336.

Oikonomou, E., Latsios, G., Vogiatzi, G. and Tousoulis, D., 2018. "Chapter 1.3 - Atherosclerotic Plaque". In D. Tousoulis, ed., *Coronary Artery Disease*, Academic Press, pp. 31–41.

Stone, G.W., Moses, J.W., Ellis, S.G., Schofer, J., Dawkins, K.D., Morice, M.C., Colombo, A., Schampaert, E., Grube, E., Kirtane, A.J., Cutlip, D.E., Fahy, M., Pocock, S.J., Mehran, R. and Leon, M.B., 2007. "Safety and Efficacy of Sirolimus- and Paclitaxel-Eluting Coronary Stents". *New England Journal of Medicine*, Vol. 356, No. 10, pp. 998–1008.

Tan, L., Wang, X., Yuan, K., Yin, T., Du, R., Shen, L., Zhu, Z., Yu, S., Zhang, H. and Wang, G., 2023. "Structural and temporal dynamics analysis on drug-eluting stents: History, research hotspots and emerging trends". *Bioactive Materials*, Vol. 23, pp. 170–186.

Tocci, G., Barbato, E., Coluccia, R., Modestino, A., Pagliaro, B., Mastromarino, V., Giovannelli, F., Berni, A. and Volpe, M., 2015. "Blood Pressure Levels at the Time of Percutaneous Coronary Revascularization and Risk of Coronary In-Stent Restenosis". *American Journal of Hypertension*, Vol. 29, No. 4, pp. 509–518.

Verdugo, F. and Badia, S., 2022. "The software design of Gridap: A Finite Element package based on the Julia JIT compiler". *Computer Physics Communications*, Vol. 276, p. 108341.

Yin, J., Li, Y., Chen, Y., Wang, C. and Song, X., 2023. "Biodegradable polymer everolimus-eluting stents versus contemporary drug-eluting stents: a systematic review and meta-analysis". *Scientific Reports*, Vol. 13, No. 1, p. 1715.

Zunino, P., 2004. "Multidimensional pharmacokinetic models applied to the design of drug-eluting stents". *Cardiovascular Engineering: An International Journal*, Vol. 4, pp. 181–191.

7. RESPONSIBILITY NOTICE

The authors are the solely responsible for the printed material included in this paper.